Interim Progress Report on NASA Grant NAG5-2232

"Receiver Design, Performance Analysis, and Evaluation for Space-Borne Laser Altimeters and Space-to-Space Laser Ranging Systems"

for the period of April 15 to October 15, 1993

Frederic M. Davidson and *Xiaoli Sun*

October 1993

Department of Electrical and Computer Engineering
The Johns Hopkins University, Baltimore, MD 21218-2686

SUMMARY

This Interim report consists of four separate reports resulted from our research on the receivers of NASA's Gravity AND Magnetic Experiment Satellite (GAMES). The first report is entitled "Analysis of phase estimation bias of GAMES Receiver due to Doppler shift." The second report is "Background radiation on GAMES fine ranging detector from the moon, the planets, and the stars." The third report is "Background radiation on GAMES receivers from the ocean sun glitter and the direct sun." The fourth report is "GAMES receiver performance versus background radiation power on the detectors."

X. Sun
June 29, 1993

Analysis of Phase Estimation Bias of GAMES Receiver due to Doppler Shift

Xiaoli Sun
The Johns Hopkins University
Baltimore, Maryland 21218-2686

The average receiver signal from an ideal photodetector may be written as

$$x_o(t) = A\cos[(\omega_c + \omega_D)t + \theta] \tag{1}$$

The actual signal into the computer is the truncated and digitized signal given in (1) and it can be written as

$$x(t) = \sum_{n=n_0}^{N+n_0} x_n \delta(t - n\Delta t) = w(t) \cdot \left(\sum_{n=-\infty}^{\infty} \delta(t - n\Delta t) \right) \cdot x_o(t) \tag{2}$$

where

$$w(t) = \begin{cases} 1, & t_o \le t \le T + t_o \\ 0, & Otherwise \end{cases}, \qquad N = \frac{\Delta t}{T} \tag{3}$$

and

$$x_n = x_o(n\Delta t) = A\cos[(\omega_c + \omega_D)n\Delta t + \theta] \tag{4}$$

The phase esitmator according to NRAO method is given by

$$\hat{\theta} = tan^{-1}\left\{ \frac{Im[X(\omega_c)]}{Re[X(\omega_c)]} \right\} = tan^{-1}\left[\frac{\sum_{n=n_o}^{N+n_o} x_n \sin(\omega_c n\Delta t)}{\sum_{n=n_o}^{N+n_o} x_n \cos(\omega_c n\Delta t)} \right] \tag{5}$$

where

$$
\begin{aligned}
X(\omega_c) &= \int_{-\infty}^{\infty} x(t) e^{-j\omega_c t} dt \\
&= \sum_{n=n_0}^{N+n_0} x_n \int_{-\infty}^{\infty} e^{-j\omega_c t} \delta(t - n\Delta t) dt \\
&= \sum_{n=n_o}^{N+n_o} x_n \cos(\omega_c n\Delta t) + j \sum_{n=n_o}^{N+n_o} x_n \sin(\omega_c n\Delta t)
\end{aligned} \tag{6}
$$

The Fourier transform of the right hand side of Eq. (2) can also be written as

$$
X(\omega) = W(\omega) * \left(\frac{2\pi}{\Delta t} \sum_{k=-\infty}^{\infty} \delta(\omega - k\frac{2\pi}{\Delta t}) \right) * X_o(\omega) \tag{7}
$$

Since

$$
W(\omega) = T \cdot \sin c\left(\frac{\omega T}{2} \right) \cdot e^{-j\omega t_o} \tag{8}
$$

and

$$
X_o(\omega) = \frac{A}{2} \left\{ e^{j\theta} \delta[\omega - (\omega_c + \omega_D)] + e^{-j\theta} \delta[\omega + (\omega_c + \omega_D)] \right\}, \tag{9}
$$

therefore

$$
\begin{aligned}
X(\omega) = \frac{\pi TA}{\Delta t} &\left\{ \sum_{k=-\infty}^{\infty} \sin c[\frac{(\omega - k\frac{2\pi}{\Delta t})T}{2}] \, e^{-j(\omega - k\frac{2\pi}{\Delta t})t_0} \right\} \\
&* \left\{ e^{j\theta} \delta[\omega - (\omega_c + \omega_D)] + e^{-j\theta} \delta[\omega + (\omega_c + \omega_D)] \right\}
\end{aligned} \tag{10}
$$

$$X(\omega)=\frac{\pi TA}{\Delta t}\left\{e^{j\theta}\sum_{k=-\infty}^{\infty}sinc\left[\frac{(\omega-(\omega_c+\omega_D)-k\frac{2\pi}{\Delta t})T}{2}\right]e^{-j(\omega-(\omega_c+\omega_D)-k\frac{2\pi}{\Delta t})t_0}\right.$$
$$\left.+e^{-j\theta}\sum_{k=-\infty}^{\infty}sinc\left[\frac{(\omega+(\omega_c+\omega_D)-k\frac{2\pi}{\Delta t})T}{2}\right]e^{-j(\omega+(\omega_c+\omega_D)-k\frac{2\pi}{\Delta t})t_0}\right\} \quad (11)$$

Assuming $\frac{2\pi}{\Delta t} >> \omega_c+\omega_D$ and filtering out all the $k \neq 0$ terms,

$$X(\omega)=\frac{\pi TA}{\Delta t}\left\{e^{j\theta}\,sinc(\frac{\omega_D T}{2})\,e^{j\omega_D t_0}\right.$$
$$\left.+e^{-j\theta}\,sinc\left[\frac{(2\omega_c+\omega_D)T}{2}\right]e^{-j(2\omega_c+\omega_D))t_0}\right\} \quad (12)$$

The phase esitmator becomes

$$\hat{\theta}=tan^{-1}\left\{\frac{Im[X(\omega_c)]}{Re[X(\omega_c)]}\right\}$$
$$=tan^{-1}\left\{\frac{sin(\omega_D t_0+\theta)sinc(\frac{\omega_D T}{2})-sin[(2\omega_c+\omega_D)t_0+\theta]sinc\left[\frac{(2\omega_c+\omega_D)T}{2}\right]}{cos(\omega_D t_0+\theta)sinc(\frac{\omega_D T}{2})+cos[(2\omega_c+\omega_D)t_0+\theta]sinc\left[\frac{(2\omega_c+\omega_D)T}{2}\right]}\right\} \quad (13)$$

If one select t_o such that $2\omega_c t_0=2m\pi$ with any integer m, then

$$sin[\theta+(2\omega_c+\omega_D)t_0]=sin(\theta+\omega_D t_0) \quad (14)$$

and

$$\hat{\theta} = tan^{-1}\left\{\frac{sin(\omega_D t_0+\theta)sinc(\frac{\omega_D T}{2}) - sin(\omega_D t_0+\theta)sinc\left[\frac{(2\omega_c+\omega_D)T}{2}\right]}{cos(\omega_D t_0+\theta)sinc(\frac{\omega_D T}{2}) + cos(\omega_D t_0+\theta)sinc\left[\frac{(2\omega_c+\omega_D)T}{2}\right]}\right\}$$

$$= tan^{-1}\left\{tan(\omega_D t_0+\theta)\cdot\frac{\frac{sin(\omega_D T/2)}{\omega_D T/2} - \frac{sin[(2\omega_c+\omega_D)T/2]}{(2\omega_c+\omega_D)T/2}}{\frac{sin(\omega_D T/2)}{\omega_D T/2} + \frac{sin[(2\omega_c+\omega_D)T/2]}{(2\omega_c+\omega_D)T/2}}\right\} \quad . \quad (15)$$

If $\omega_c T = 2n\pi$ for any integer n, $sin[\frac{(2\omega_c+\omega_D)T}{2}] = sin(\frac{\omega_D T}{2})$ and

$$\hat{\theta} = tan^{-1}\left\{tan(\omega_D t_0+\theta)\cdot\frac{\frac{1}{\omega_D} - \frac{1}{(2\omega_c+\omega_D)}}{\frac{1}{\omega_D} + \frac{1}{(2\omega_c+\omega_D)}}\right\} \quad (16)$$

$$= tan^{-1}\left\{tan(\omega_D t_0+\theta)\cdot\frac{\omega_c}{\omega_c+\omega_D}\right\}$$

The largest estimation error occurs when the argument of the tan^{-1} function is near zero. Under this condition, $tan^{-1}(x) \approx x$ and $tan(x) \approx x$, the relative bias, ε, of the NRAO estimator (5) is given by

$$\varepsilon = \frac{1}{\omega_D t_0+\theta}\cdot E\left\{\hat{\theta} - (\omega_D t_0+\theta)\right\} \le -\frac{\omega_D}{\omega_c+\omega_D} \approx -\frac{\omega_D}{\omega_c}, \qquad (\omega_D << \omega_c) \quad (17)$$

An unbiased phase estimator is given by

$$\hat{\theta} = tan^{-1}\left[\left(1-\frac{\omega_D}{\omega_c+\omega_D}\right)\frac{\sum_{n=n_o}^{N+n_o} x_n sin(\omega_c n\Delta t)}{\sum_{n=n_o}^{N+n_o} x_n cos(\omega_c n\Delta t)}\right]. \quad (18)$$

where x_n is given by (4).

Background Radiation on GAMES Fine Ranging Detector from the Moon, the Planets, and Stars

X. Sun/JHU

Rev. 1, October 1993

The moon, the planets and stars also contribute to the background radiation when they are close to the GAMES telescope axis. The angles they subtend are rather small, with the largest being equal to about 0.5° by the moon. Therefore, we can treat them as point sources when calculating their contributions to the background radiation noise on the GAMES fine ranging detector. The corresponding background power of each object is then given by

$$P_b = E_\lambda \Delta\lambda \frac{\pi D_{tel}^2}{4} R_{OA}(\theta_{OA}) \tag{1}$$

where E_λ is the spectral irradiance of the object, $\Delta\lambda$ is the optical bandwidth, D_{tel} is the telescope diameter, θ_{OA} is the angle between the object and the telescope axis, and $R_{OA}(\theta_{OA})$ is the telescope off-axis rejection ratio at θ_{OA}.

The values of $R_{OA}(\theta_{OA})$ were provided by Kimberly Mehalick of Advanced Technology & Research Corp. using the computer program package called Mini-Apart [1]. The smallest off-axis angle had to be greater than the FOV of the GAMES tracking system, i.e., 0.60 degrees (10.5 mrad). The value of $R_{OA}(\theta_{OA})$ at 0.6 degrees was about -57 dB for baffle lengths from 400 mm to 630 mm. Use of longer baffle lengths greatly reduces the stray light at relatively large off-axis angle but not just at a few degrees.

Table 1 lists the values of E_λ at λ=800 nm, the power on the fine ranging detector when $\theta_{OA} = 0°$, and the power of the stray light on the GAMES fine ranging receiver from the moon, the planets, and bright stars. The values of E_λ were obtained from References [2] and [3] when the objects are at their brightest when looking from the

earth. The telescope diameter is taken to be 20 cm, the optical bandwidth 3.9 nm, and the baffle length 400 mm, 515 mm, and 630 mm.

It has been shown that the GAMES fine ranging receiver is not significantly affected by the stray light if the total noise power at the detector does not exceed 1.0 pW. The sun and sun lit cloud are the primary sources of stray light. Therefore, the moon, the planets, and stars may be neglected when considering the total stray light on the detector if those objects are not within the GAMES tracking receiver FOV (20×20 mrad).

The amount of background radiation noise on the GAMES tracking CCD array due to these objects can be scaled from those in Table 1 and the scaling factor is equal to the square of the ratio of the field of views.

Objects	E_λ $(W/m^2/nm)$	$P_b(\theta_{OA}=0)$ (W)	$P_b(\theta_{OA}=10.5$ mrad) (W)		
			400mm	515mm	630mm
Moon	4.0×10^{-6}	5.0×10^{-7}	9.55×10^{-13}	9.53×10^{-13}	9.44×10^{-13}
Venus	1.0×10^{-9}	1.3×10^{-10}	2.48×10^{-16}	2.48×10^{-16}	2.45×10^{-16}
Mars	2.0×10^{-10}	2.5×10^{-11}	4.78×10^{-17}	4.76×10^{-17}	4.72×10^{-17}
Jupiter	2.0×10^{-10}	2.5×10^{-11}	4.78×10^{-17}	4.76×10^{-17}	4.72×10^{-17}
Saturn	1.0×10^{-10}	1.3×10^{-11}	2.48×10^{-17}	2.48×10^{-17}	2.45×10^{-17}
Mercury	3.0×10^{-11}	3.8×10^{-12}	7.26×10^{-18}	7.24×10^{-18}	7.17×10^{-18}
Sirius	4.0×10^{-11}	5.0×10^{-12}	9.55×10^{-18}	9.53×10^{-18}	9.44×10^{-18}
Betelgeux	3.0×10^{-11}	3.8×10^{-12}	7.26×10^{-18}	7.24×10^{-18}	7.17×10^{-18}
Arcturus	3.0×10^{-11}	3.8×10^{-12}	7.26×10^{-18}	7.24×10^{-18}	7.17×10^{-18}
Crucis	3.0×10^{-11}	3.8×10^{-12}	7.26×10^{-18}	7.24×10^{-18}	7.17×10^{-18}
Canopus	2.5×10^{-11}	3.8×10^{-12}	7.26×10^{-18}	7.24×10^{-18}	7.17×10^{-18}
Antares	2.0×10^{-11}	2.5×10^{-12}	4.78×10^{-18}	4.76×10^{-18}	4.72×10^{-18}
Pollux	1.2×10^{-11}	1.5×10^{-12}	2.87×10^{-18}	2.86×10^{-18}	2.83×10^{-18}
Vega	1.0×10^{-11}	1.3×10^{-12}	2.48×10^{-18}	2.48×10^{-18}	2.45×10^{-18}
β Gruis	1.0×10^{-11}	1.3×10^{-12}	2.48×10^{-18}	2.48×10^{-18}	2.45×10^{-18}
Achernar	7.0×10^{-12}	8.9×10^{-13}	1.70×10^{-18}	1.70×10^{-18}	1.68×10^{-18}
Rigal	5.0×10^{-12}	6.3×10^{-13}	1.20×10^{-18}	1.20×10^{-18}	1.19×10^{-18}

Table 1

References

[1] A. W. Greynolds, "Formulas for estimating stray-radiation levels in well-baffled optical systems," in *Radiation Scattering in Optical Systems*, SPEI Proceedings, Vol. 257, pp. 39-49, 1980.

[2] *The Infrared & Electro-Optical Systems Handbook*, Volume 1 *Sources of Radiation*, G. J. Zissis, Editor, SPIE Press, Bellingham, Washington, 1993, p. 163.

[3] *Electro-Optics Handbook*, RCA Corp., Technical Series EOH-11, Lancaster, PA, 1974, pp. 67-68.

Background Radiation on GAMES Receivers from the Ocean Sun Glitter and the Direct Sun

The derivation given below proofs that the sun glitter light always enter the GAMES telescope at a larger incident angle than the direct sun light. In other words, the attenuation of the telescope to the sun glitter is always greater than the attenuation to the much brighter direct sun light. One needs only consider the effect of the direct sun when analyzing the total background noise radiation on the GAMES detector from the sun.

We assumed in the derivation that the sun is a distant point source and the ocean is calm as a mirror. In practice, the sun is an extended source which subtends about 0.5 degree. Nevertheless, it can be considered to be composed of point sources and our derivation still apply. The actual sea surface always has waves that the sun glitter from the ocean is fuzzier and larger than what would be reflected from the calm ocean. However, total energy of the solar irradiance onto the earth is constant and the reflected sun light energy should be distributed more evenly over the hemisphere due to the roughness of the sea. Therefore, the total light entering the telescope from the sun glitter should not increase due to the roughness of the sea.

The earth atmosphere and clouds also attenuate the sun glitter and makes it even less important as compared to the direct sun.

Figure S1 shows the geometry of the direct sun light and the reflection from the ocean. The sun light is assumed to come from a point source at infinity and can be considered as parallel beams. The GAMES telescope is pointing downward at an angle $\gamma + \pi/2$ with respect to the zenith. The earth radius is r and the telescope altitude is h. The telescope axis is given by the vector $\vec{n}$. We only consider the case where all the angles labeled in Figure S1 are smaller than $\pi/2$.

We claim that the incident angle of the direct sun light is smaller than that of the

reflected sun light, i.e. $\alpha < \beta$ for small γ.

We first derive the relationship between the angles ϕ and λ. From the basic law of reflection and trigonometry,

$$\left(\frac{\pi}{2} + \psi\right) + \omega + \lambda = \pi \tag{1}$$

$$\left(\frac{\pi}{2} - \psi\right) + (\pi - \varphi) + \omega = \pi \tag{2}$$

Eliminate ω

$$\psi = \frac{1}{2}(-\lambda - \varphi + \pi) \tag{3}$$

From the Theorem of Sine

$$\frac{\sin(\lambda)}{r} = \frac{\sin\left(\frac{\pi}{2} + \psi\right)}{r + h} \tag{4}$$

Solve for ψ

$$\psi = \arcsin\left(\frac{[h + r]\sin[\lambda]}{r}\right) - \frac{1}{2}\pi \tag{5}$$

Substitute (3) into (??) and solve for ϕ

$$\varphi = -2\left(\arcsin\left[\frac{\{h + r\}\sin\{\lambda\}}{r}\right] - \frac{1}{2}\pi\right) - \lambda + \pi \tag{6}$$

Since $\sin(\theta) = \sin(\pi - \theta)$, $\arcsin(x) = \pi - \arcsin(x)$, Equation (6) can be rewritten as

$$\varphi = -2\left(\left[\pi - \arcsin\left\{\frac{(h + r)\sin(\lambda)}{r}\right\}\right] - \frac{1}{2}\pi\right) - \lambda + \pi$$

$$\varphi = 2\arcsin\left(\frac{[h + r]\sin[\lambda]}{r}\right) - \lambda \tag{7}$$

Figure S2 shows a plot of λ vs. ϕ for the earth radius r=*6370 km* and GAMES altitude r =*250 km* .

The relationship between the angles α and β is given by the following two equations

$$\beta = \frac{\pi}{2} - \lambda - \gamma \tag{8}$$

$$\alpha = \frac{\pi}{2} - \varphi + \gamma \tag{9}$$

Eliminate the variable λ and substitute Equation (6) for φ,

$$\alpha = -2 \arcsin \left(\frac{[h + r] \sin \left[-\gamma - \beta + \frac{1}{2}\pi \right]}{r} \right) - \beta + \pi \qquad (10)$$

Plots of β vs. α are shown in Figures S3, S4, and S5 for $\gamma = 0$, $0.86°$, and $45°$, respectively. It is seen that α is always smaller than β for $\gamma = 0$. For $\gamma = 0.86°$, which is about the worst case for GAMES, $\alpha < \beta$ for at least $\alpha < 1$ rad ($\sim 57°$). We need not consider the case for $\alpha > 1$ rad because the sun lit clouds become dominate for such sun angles.

Sun glitter would become significant if the telescope were pointed down at the earth, for example $\gamma = 45°$. The relationship $\alpha > \beta$ would no longer hold, as shown in Figure S5.

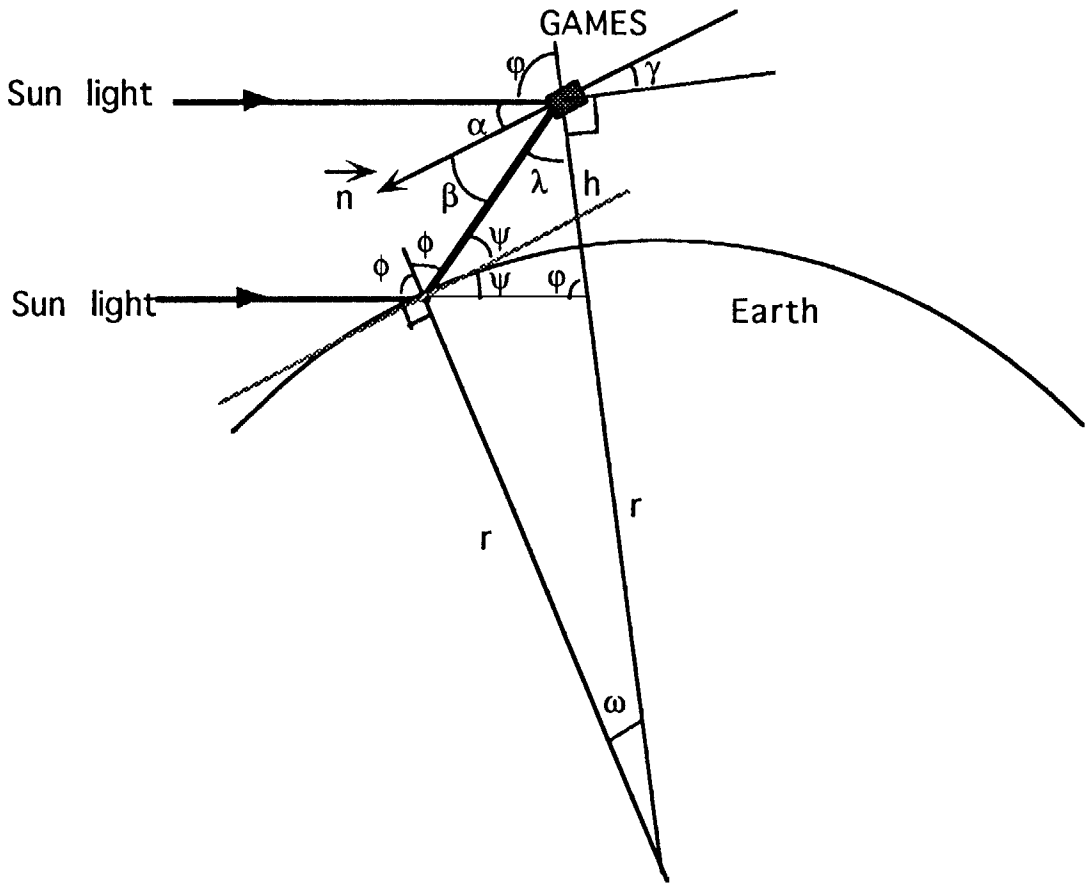

Figure S1. The geometry of the direct sun light and the reflected sun light.

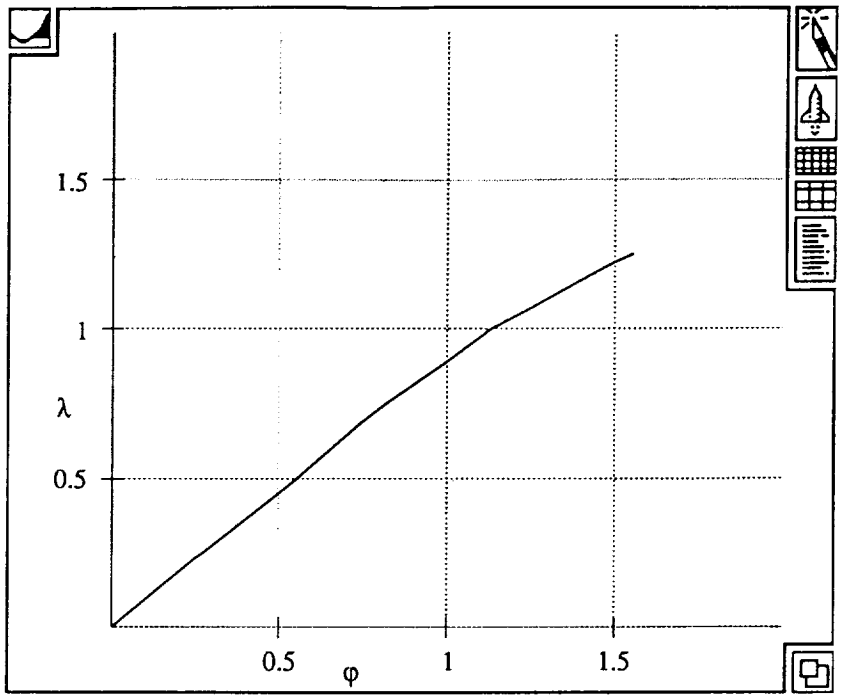

Figure S2

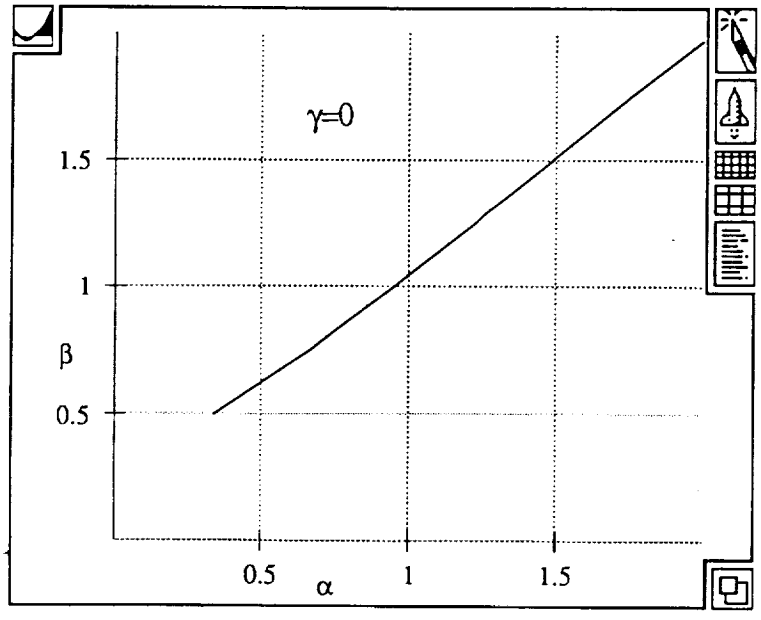

Figure S3

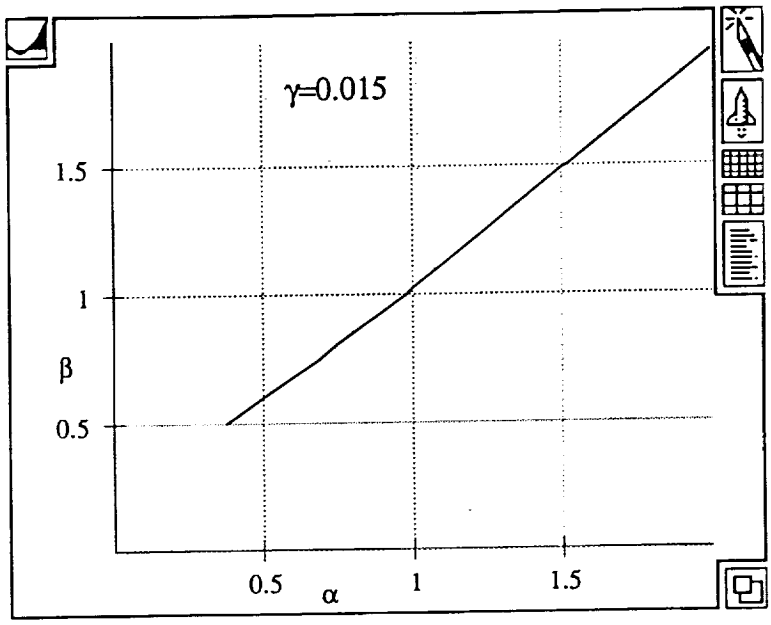

Figure S4

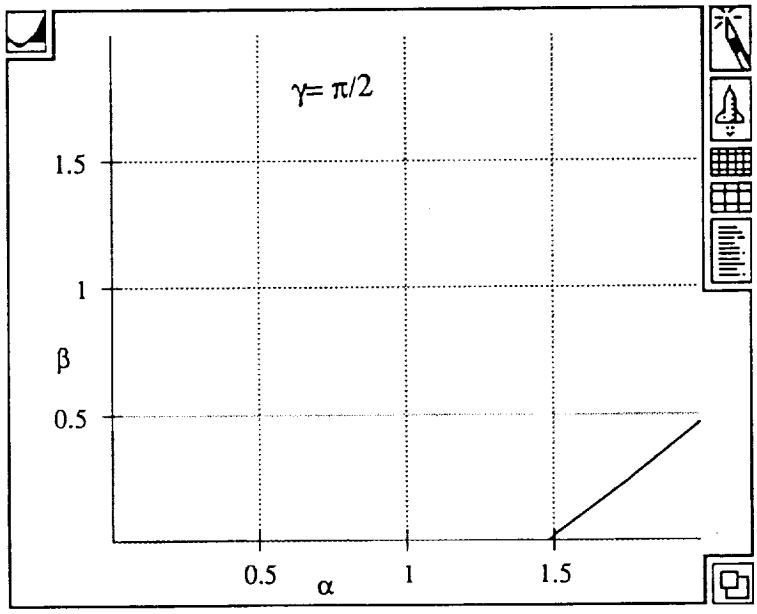

Figure S5

GAMES Receiver Performance versus Background Radiation Power on the Detectors

Figure 14 shows the calculated rms ranging error per second as function of background radiation powers incident on the PMT. Figure 15 shows the rms ranging error versus the sun angle for 400mm, 515mm, and 630mm baffle length. All the system parameters and the numerical results are given in the attached spread sheets. It is shown that the background radiation power on the PMT should be kept below 1.0 pW, which is about equal to the equivalent noise power due to the PMT dark current and the non ideal laser transmitter on-off extinction ratio (80

Figures 16 and 17 show the performance of the CCD tracking detector vs. the total background radiation power and sun angles, respectively. The tracking detector was assumed to have a FOV 10 times that of the fine ranging detector. The CCD was assumed to have 512 by 512 pixels and the tracking beacon illuminated 4 pixels. All the system parameters and the numerical results are given in the attached spread sheets.

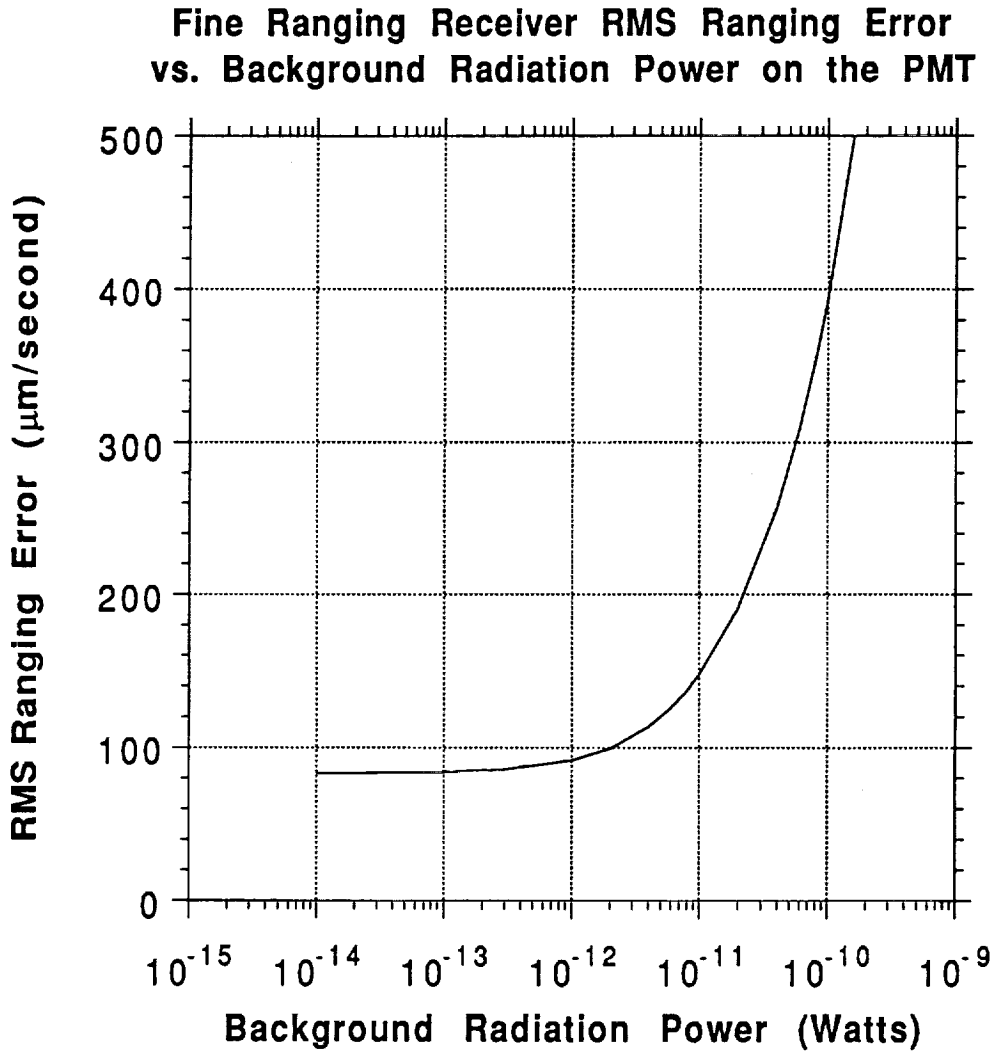
Fine Ranging Receiver RMS Ranging Error
vs. Background Radiation Power on the PMT
RMS Ranging Error (μm/second)
500
400
300
200
100
0
10-15
10-14
10-13
10-12
10-11
10-10
10-9
Background Radiation Power (Watts)

Fine Ranging Receiver RMS Error vs. Sun Angle

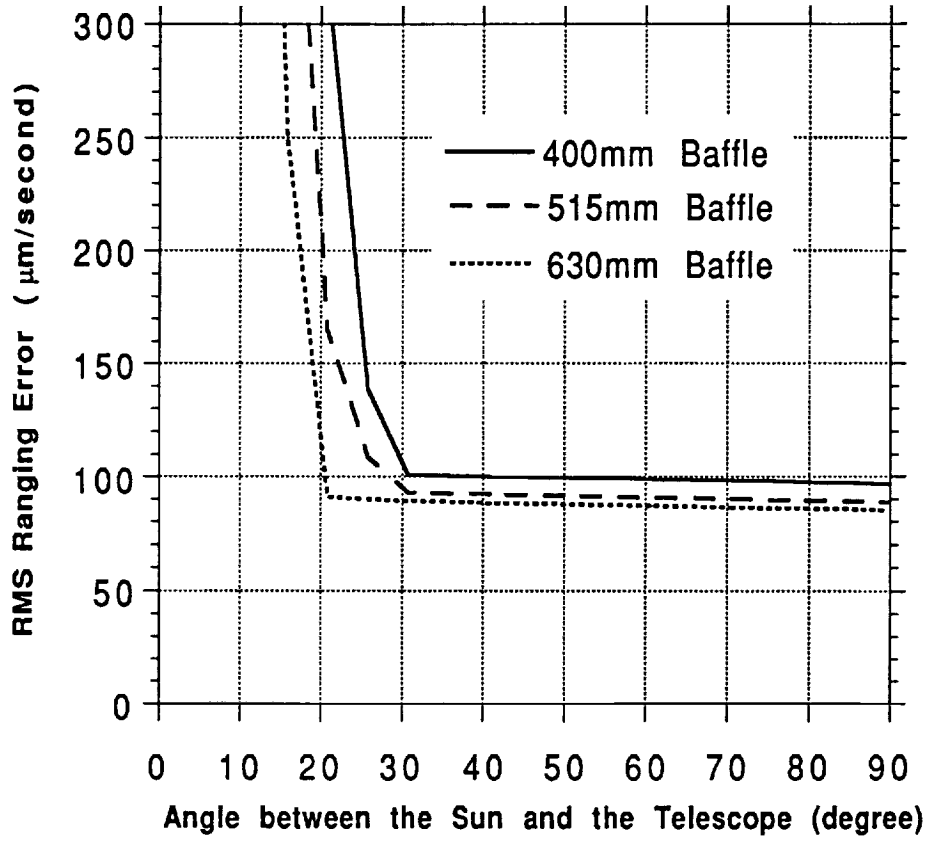

Tracking Receiver SNR/pixel/frame versus Background Radiation Power over Full FOV

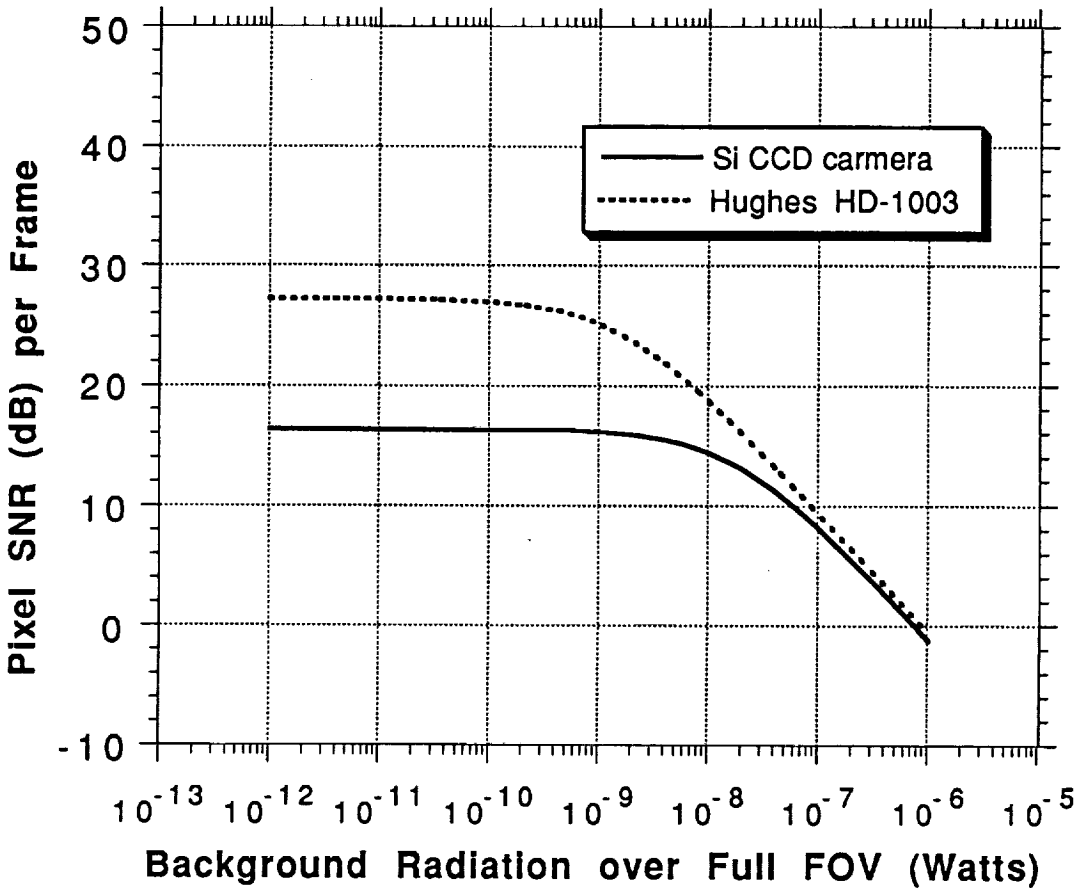

Tracking Receiver SNR/pixel/frame versus Sun Angle for Baffle length 400, 515, and 630 mm

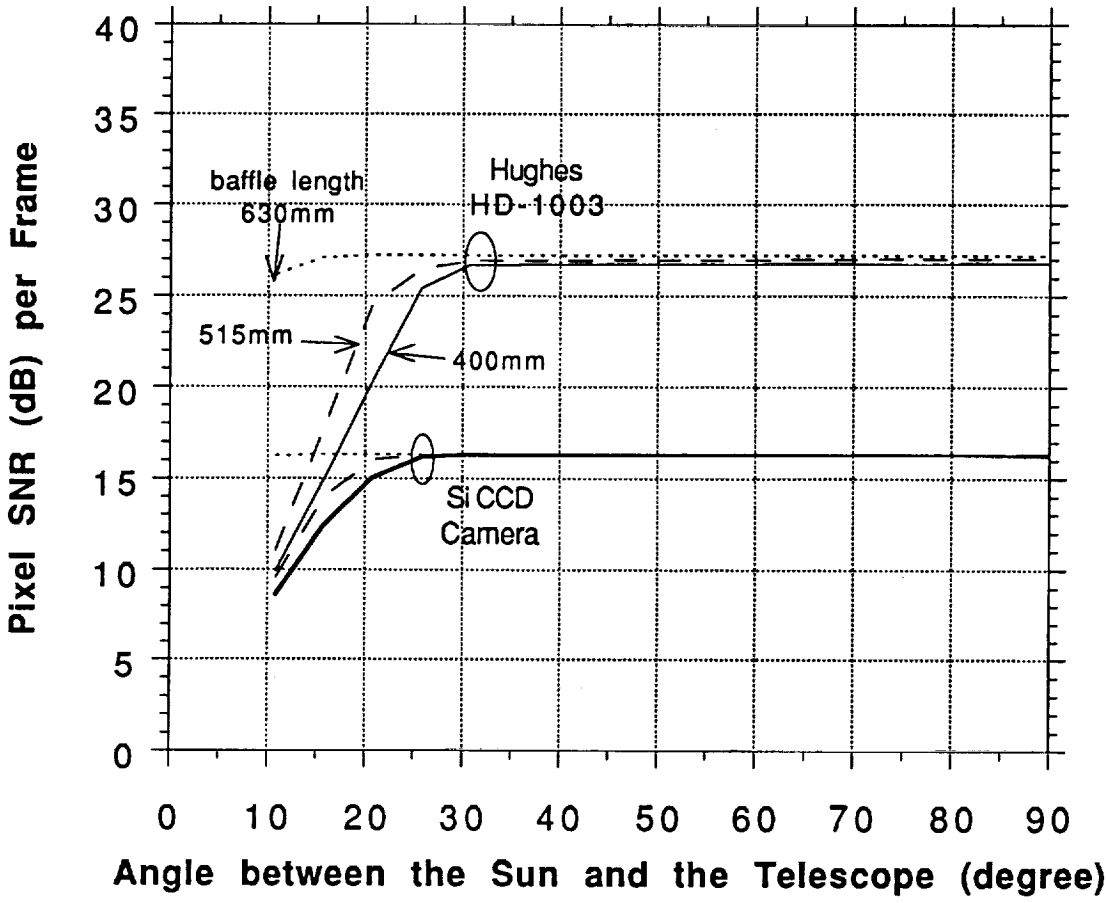

GAMES Fine Ranging Performance Calculations

Xiaoli Sun, Johns Hopkins University

		Comments
1. Range Calculation		
a. Earth Radius (km)	6370	
b. Orbit Altitude (km)	300	
c. Range to subsatellite (km)	**200**	
d. Signal roundtrip time (msec)	1.33	
2. Laser Transmitter		
a. Signal wavelength (nm)	845	
b. Photon energy (J)	2.35E-19	
c. Xmit Beam Width (mrad)	**1.00**	
d. Laser diode Xmit power (mW)	**60.0**	
e. Alloc. link loss Margin (dB)	**9.00**	
f. Xmit Power reduced by alloc. margin (mW)	7.55	
g. Laser Modulation Index (0 - 1.0)	0.80	*Practical AlGaAs Transmitter*
h. Modulation frequency (MHz)	**2000**	
i. Range per Modulation Period (mm)	75.0	
j. Unmodulated transmitter power (mW)	1.511	*Leakage when laser is "off"*
k. Range resol. per deg. in phase (um)	208	
3. Pointing Calculation		
a. Drive motor steps/revolution	131,072	*17 bit encoder controlled to ± 1 bit*
b. Motor urad/step	47.94	*Precision mount not req'd*
c. Motor steps/beam width	20.86	
4. Target Calculations		
a. CC diameter (cm)	**8.00**	
b. CC area (m^2)	5.03E-03	
5. CC Velocity Aberration Calculations		
a. CC diffr. limit FWHM angle (urad)	12.89	
b. Satellite Tang. velocity (km/sec)	7.00	*Approximate*
c. Angle below horizon to subsatellite (deg)	0.86	
d. Dist. change of Main s/c dur. prop time (m)	9.33	
e. Perp. Angular motion of main spacecraft (urad)	0.70	
f. Fraction of angular width of CC diffr. pattern	0.05	
6. Rcvd Signal Calc's ("top hat" beam)		
a. Telescope diameter (cm)	**20.00**	
b. Transmitter & receiver transmission	**0.50**	
c. Telescope area (6cm cent obsc) (m^2)	2.86E-02	
d. Laser spot diameter at subsatellite (m)	200.00	
e. Laser spot area at subsatellite (m^2)	3.14E+04	
f. Fraction of laser energy captured by cc's	1.60E-07	
g. Area of CC laser return at GAMES (m^2)	5.22	
h. Fraction of cc signal captured by telescope	5.48E-03	
i. Total Signal transmission factor to ranging det.	4.38E-10	
k. Detected ranging signal power (watts)	2.65E-12	

l. Ranging signal rate (photons/sec)	1.13E+07		
m. Unmodulated signal leakage (photons/sec)	2.82E+06		
n. Background radiation noise (Watts)	**2.5E-13**		
o. Background radiation noise (photon/sec)	1.06E+06		
7. PMT Detector Parameters	**at Anode**	**Cathode**	**in pe/sec**
a. PMT Quantum Efficiency	**0.100**	*GaAs photocathod*	
b. PMT Gain	**1.0E+05**		
c. PMT Dark Current (amps)	**1.0E-09**	1.0E-14	6.3E+04
d. Background Current (amps)	1.7E-09	1.7E-14	1.1E+05
e. Det. unmodulated signal leakage (amps)	4.5E-09	4.5E-14	2.8E+05
f. Total average PMT Noise Current (amps)	7.21E-09	7.21E-14	4.51E+05
g. Det. Ranging signal (amps)	1.80E-08	1.80E-13	1.13E+06
h. PMT Excess Noise Factor (F)	**1.50**	*Likely to be better (≈1.3)*	
i. PMT rms timing jitter (psec)	**40.0**		
j. Signal Power Loss due to Timing Jitter	0.78		
j. Signal Power Loss due to Timing Jitter (dB)	-1.1		
k. Electron Charge (Coulombs)	1.60E-19		
l. Preamp Noise current Density (pA/Hz^1/2)	**20.0**		
8. Receiver Parameters			
a. Receiver Bandwidth (Hz)	200		
b. Noise Bandwidth (Hz)	400		
9. PLL Receiver Performance	**at Anode**	**Cathode**	**in pe/sec**
a. Average Signal Current (amps)	1.59E-08	1.59E-13	9.93E+05
b. Signal Power (A^2)	1.26E-16	1.26E-26	4.93E+11
c. PMT Sig. Shot Noise Variance (amps^2)	3.46E-19	3.46E-29	1.35E+09
d. Dark Current Noise Variance (amps^2)	1.92E-20	1.92E-30	7.50E+07
e. Backgnd Noise Variance (amps^2)	3.27E-20	3.27E-30	1.28E+08
f. Sig. Leak. Noise Variance (amps^2)	8.66E-20	8.66E-30	3.38E+08
g. Preamplifier Noise Current Variance	1.60E-19	1.60E-29	6.25E+08
h. Total PMT Noise Current Variance (amps^2)	6.45E-19	6.45E-29	2.52E+09
i. SNR	1.96E+02		
j. SNR (dB)	22.92		
k. Root SNR	***14.00***		
10. Ranging Performance			
a. Phase Estimator Variance (rad^2)	2.55E-03		
b. rms Phase Estimation Error (mrad)	50.52		
c. rms Phase Estimation Error (deg)	2.89		
d. rms Ranging Error per Measurement (um)	603		
e. rms Range Error per sec (um)	***42.6***		
f. Actual Range Error (um)	85.3	*twice the calculated ones*	

g. Required max range error per sec (um)	**50.0**
h. Minimum SNR required	1.42E+02
i. Minimum SNR required (dB)	21.5
k. Laser Power Link Margin (dB)	***1.8***

Background Radiation Power (Watts)	RMS Ranging Error (um)
	85.28
1.00E-14	83.18
3.00E-14	83.35
1.00E-13	83.97
3.00E-13	85.71
1.00E-12	91.53
2.00E-12	99.26
4.00E-12	113.14
6.00E-12	125.50
8.00E-12	136.74
1.00E-11	147.13
2.00E-11	190.76
4.00E-11	256.66
6.00E-11	308.81
8.00E-11	353.34
1.00E-10	392.85
2.00E-10	549.33
4.00E-10	772.42
6.00E-10	944.19
8.00E-10	1089.20
1.00E-09	1217.05
3.00E-09	2104.71
1.00E-08	3840.57

Baffel Length 400 mm

Sun Angle to telescope (degrees)	Background noise power (Watts)	RMS Ranging Error (um/s)
		85.28
10.86	8.79E-10	1141.41
15.86	2.61E-10	625.86
20.86	6.38E-11	317.75
25.86	8.31E-12	138.40
30.86	2.19E-12	100.66
35.86	2.11E-12	100.07
40.86	2.05E-12	99.63
45.86	2.03E-12	99.48
50.86	1.99E-12	99.18
55.86	1.97E-12	99.03
60.86	1.94E-12	98.81
65.86	1.90E-12	98.51
70.86	1.85E-12	98.14
75.86	1.79E-12	97.69
80.86	1.74E-12	97.31
85.86	1.70E-12	97.00
90.86	1.59E-12	96.16

Baffel Length 515 mm

Sun Angle to telescope (degrees)	Background noise power (Watts)	RMS Ranging Error (um/s)
		85.28
10.86	6.70E-10	997.34
15.86	1.28E-10	442.28
20.86	1.38E-11	165.07
25.86	3.28E-12	108.35
30.86	1.17E-12	92.89
35.86	1.10E-12	92.33
40.86	1.04E-12	91.85
45.86	9.99E-13	91.52
50.86	9.60E-13	91.21
55.86	9.18E-13	90.87
60.86	8.79E-13	90.55
65.86	8.33E-13	90.18
70.86	7.90E-13	89.82
75.86	7.37E-13	89.39
80.86	6.97E-13	89.06
85.86	6.66E-13	88.80
90.86	5.91E-13	88.17

Baffel Length 630 mm

Sun Angle to telescope (degrees)	Background noise power (Watts)	RMS Ranging Error (um/s)
		85.28
10.86	4.62E-10	829.48
15.86	3.79E-11	250.56
20.86	9.26E-13	90.93
25.86	7.96E-13	89.87
30.86	6.93E-13	89.02
35.86	6.36E-13	88.55
40.86	5.87E-13	88.14
45.86	5.43E-13	87.77
50.86	5.04E-13	87.44
55.86	4.64E-13	87.11
60.86	4.27E-13	86.79
65.86	3.85E-13	86.44
70.86	3.46E-13	86.10
75.86	3.02E-13	85.72
80.86	2.71E-13	85.46
85.86	2.47E-13	85.25
90.86	1.91E-13	84.76

GAMES Tracking System Performance Calculations

6/18/93 by Xiaoli Sun

		Comments
1. Range Calculation		
a. Earth Radius (km)	6370	
b. Orbit Altitude (km)	300	
c. Range to subsatellite (km)	**200**	
d. Signal roundtrip time (msec)	1.33	
2. Laser Transmitter		
a. Signal wavelength (nm)	845	
b. Photon energy (J)	2.35E-19	
c. Xmit Beam Width (mrad)	**10.00**	*1/2 degree beamwidth*
d. Actual Xmit power (mW)	**60**	*Single SDL 5410 laser diode*
e. Total alloc. link loss (dB)	**9.00**	*Itemized on a seperate sheet*
d. Xmit Power reduced by alloc. margin (mW)	**8**	
3. Pointing Calculation		
a. Drive motor steps/revolution	131,072	*17 bit encoder controlled to ± 1 bit*
b. Motor urad/step	47.9	*Precision mount not req'd*
c. Motor steps/beam width	208.6	
4. Target Calculations		
a. CC diameter (cm)	**8.00**	
b. CC area (m^2)	5.03E-03	
c. Number of cc's	1	
5. CC Velocity Aberration Calculations		
a. CC diffr. limit FWHM angle (urad)	12.89	
b. Satellite Tang. velocity (km/sec)	7.00	*Approximate*
c. Angle below horizon to subsatellite (deg)	0.86	
d. Dist. change, Main spacecraft dur. prop time (m)	9.33	
e. Perp. Angular motion of main spacecraft (urad)	0.70	
f. Fraction of angular width of CC diffr. pattern	0.05	
6. Rcvd Signal Calculations ("top hat" beam)		
a. Telescope diameter (cm)	**20.00**	
b. Transmitter & receiver transmission	0.50	
c. Telescope area (6.0 cm cent. obsc.), (m^2)	2.86E-02	
d. Laser spot diameter at subsatellite (m)	2000.00	
e. Laser spot area at subsatellite (m^2)	3.14E+06	
f. Fraction of laser energy captured by cc's	1.60E-09	
g. Area of CC laser return at Games Sat. (m^2)	5.22	
h. Fraction of cc signal captured by telescope	5.48E-03	
j. Total Signal transmission factor to tracking det.	4.38E-12	
k. Laser signal density from subsatellite (W/m^2)	2.32E-12	*(5th mag. stars ~2.0e-12 W/m^2/nm)*
k. Detected tracking signal power (watts)	3.31E-14	

7. Tracking Detector Parameters (at room temp)	Si CCDs (commericial)	Hughes HD-1003	Ball CT600
a. Quantum Efficiency	0.40	0.35	0.25
b. Pixel size (um)	27	15	27
c. Number of pixels in each dimension	512	512	512
d. Device Dark Current (pA/cm^2)	1.00E+03	25.00	1.00E+02
e. Dark electrons/pixel/sec	4.56E+04	3.52E+02	4.56E+03
f. rms Read noise (electrons)	200	50	50
g. Pixel saturation level (electrons)	3.00E+05	3.00E+05	3.00E+05
h. Max frame rate (Hz)	15	30	40
i. Power consumption (Watts)	2+more	11	7.5

8. Tracking Performance		
a. Readout rate (Hz)	10	
b. Observation time (sec)	0.10	
c. Spot size (pixels)	4	
d. Required tracking accuracy (mrad)	0.10	*1% Fine ranging beam width*
e. Resolution (mrad/pixel)	0.10	*Assume no subpixel signal processing*
f. Total background radiation power	**1.00E-09**	
g. Number of pixels of the CCD array (nXn)	**256**	
h. Background radiation power/pixel (Watts/pixel)	**1.53E-14**	
i. Background radiation (photons/pixel/sec)	6.49E+04	
j. Required noise equivalent angle (mrad)	<<0.10	

	Si CCDs (commericial)	Hughes HD-1003	Ball CT600
h. Detected signal per frame per pixel (pe)	1.41E+03	1.23E+03	8.81E+02
i. Background noise per frame (pe/pixel)	2.60E+03	2.27E+03	1.62E+03
j. Detector dark noise per frame (pe/pixel)	4.56E+03	3.52E+01	4.56E+02
k. CCD read noise electron variance	4.00E+04	2.50E+03	2.50E+03
l. Total noise electrons variance per pixel	4.86E+04	6.04E+03	5.46E+03
m. Pixel SNR (dB) per frame	16.1	25.2	21.5

9. Signal to Noise Ratio and Link Margin		
o. Minimum SNR required (dB)	15.0	*Prob(wrong pixel) < 10^-4*
p. Minimum SNR required	31.6	*NEA << 0.1 mrad (1 pixel)*

r. Minimum rcvred signal req'ed (pe/pixel/frame)	1.24E+03	4.06E+02	3.97E+02
p. Link margin in laser power (dB)	0.6	4.8	3.5

Pixel SNR (dB)

Total background radiation power (W)	Si CCDs (commericial)	Hughes HD-1003
	16.12	25.17
1.00E-12	16.35	27.21
3.00E-12	16.35	27.21
1.00E-11	16.35	27.19
3.00E-11	16.35	27.14
1.00E-10	16.33	26.96
2.00E-10	16.31	26.72
4.00E-10	16.26	26.28
6.00E-10	16.21	25.88
8.00E-10	16.16	25.51
1.00E-09	16.12	25.17
2.00E-09	15.89	23.78
4.00E-09	15.47	21.89
6.00E-09	15.09	20.57
8.00E-09	14.73	19.56
1.00E-08	14.41	18.75
2.00E-08	13.07	16.06
4.00E-08	11.22	13.22
6.00E-08	9.93	11.51
8.00E-08	8.93	10.29
1.00E-07	8.13	9.34
3.00E-07	3.81	4.62
1.00E-06	-1.24	-0.59

Baffel Length 400 mm

Sun Angle to telescope (degrees)	Total noise power (Watts)	pixel SNR CCDs (dB)	pixel SNR Star tracker (dB)
		16.12	25.17
10.86	8.79E-08	8.60	9.89
15.86	2.61E-08	12.42	14.98
20.86	6.38E-09	15.02	20.36
25.86	8.31E-10	16.15	25.45
30.86	2.19E-10	16.30	26.68
35.86	2.11E-10	16.30	26.70
40.86	2.05E-10	16.30	26.71
45.86	2.03E-10	16.30	26.72
50.86	1.99E-10	16.31	26.72
55.86	1.97E-10	16.31	26.73
60.86	1.94E-10	16.31	26.74
65.86	1.90E-10	16.31	26.75
70.86	1.85E-10	16.31	26.76
75.86	1.79E-10	16.31	26.77
80.86	1.74E-10	16.31	26.78
85.86	1.70E-10	16.31	26.79
90.86	1.59E-10	16.32	26.82

Baffel Length 515 mm

Sun Angle to telescope (degrees)	Total noise power (Watts)	pixel SNR CCDs (dB)	pixel SNR Star tracker (dB)
		16.12	25.17
10.86	6.70E-08	9.55	11.05
15.86	1.28E-08	13.99	17.81
20.86	1.38E-09	16.03	24.59
25.86	3.28E-10	16.27	26.43
30.86	1.17E-10	16.33	26.92
35.86	1.10E-10	16.33	26.94
40.86	1.04E-10	16.33	26.95
45.86	9.99E-11	16.33	26.96
50.86	9.60E-11	16.33	26.97
55.86	9.18E-11	16.33	26.98
60.86	8.79E-11	16.33	26.99
65.86	8.33E-11	16.33	27.00
70.86	7.90E-11	16.33	27.01
75.86	7.37E-11	16.34	27.03
80.86	6.97E-11	16.34	27.04
85.86	6.66E-11	16.34	27.05
90.86	5.91E-11	16.34	27.06

Baffel Length 630 mm

Sun Angle to telescope (degrees)	Total noise power (Watts)	pixel SNR CCDs (dB)	pixel SNR Star tracker (dB)
		16.12	25.17
10.86	4.62E-10	16.24	26.15
15.86	3.79E-11	16.34	27.12
20.86	9.26E-13	16.35	27.21
25.86	7.96E-13	16.35	27.21
30.86	6.93E-13	16.35	27.22
35.86	6.36E-13	16.35	27.22
40.86	5.87E-13	16.35	27.22
45.86	5.43E-13	16.35	27.22
50.86	5.04E-13	16.35	27.22
55.86	4.64E-13	16.35	27.22
60.86	4.27E-13	16.35	27.22
65.86	3.85E-13	16.35	27.22
70.86	3.46E-13	16.35	27.22
75.86	3.02E-13	16.35	27.22
80.86	2.71E-13	16.35	27.22
85.86	2.47E-13	16.35	27.22
90.86	1.91E-13	16.35	27.22